Mercury-Bridged Transition-Metal Clusters. 5.† Synthesis and Structure of $(\mu_3\text{-}\eta^2\text{-}C_2\text{-}t\text{-}Bu)(CO)_9M_3(\mu_3\text{-}Hg)M'$ [M = Ru, Os; M' = $Fe(\eta^5\text{-}C_5H_5)(CO)_2$, $Ru(\eta^5\text{-}C_5H_5)(CO)_2$, $Mo(\eta^5\text{-}C_5H_5)(CO)_3$, $Co(CO)_4$] and $[(\mu\text{-}H)(\mu_3\text{-}S)(CO)_9Os_3]_2(\mu_4\text{-}Hg)$

Edward Rosenberg,* Kenneth I. Hardcastle,* Michael W. Day, Roberto Gobetto,‡ Sharad Hajela, and Rosy Muftikian

Department of Chemistry, California State University, Northridge, California 91330

Received June 13, 1990

The synthesis and solid-state structures of $(\mu_3\text{-}\eta^2\text{-}C_2\text{-}t\text{-}Bu)(CO)_9Ru_3(\mu_3\text{-}Hg)Ru(\eta^5\text{-}C_5H_5)(CO)_2$ (**1**), $(\mu_3\text{-}\eta^2\text{-}C_2\text{-}t\text{-}Bu)(CO)_9Ru_3(\mu_3\text{-}Hg)Fe(\eta^5\text{-}C_5H_5)(CO)_2$ (**2**), $(\mu_3\text{-}\eta^2\text{-}C_2\text{-}t\text{-}Bu)(CO)_9Os_3(\mu_3\text{-}Hg)Mo(\eta^5\text{-}C_5H_5)(CO)_3$ (**3**), $(\mu_3\text{-}\eta^2\text{-}C_2\text{-}t\text{-}Bu)(CO)_9Os_3(\mu_3\text{-}Hg)Co(CO)_4$ (**4**), and $[(\mu\text{-}H)(\mu_3\text{-}S)(CO)_9Os_3]_2(\mu_4\text{-}Hg)$ (**6**) are reported. The structures are compared to known analogues with regard to their mercury–transition-metal bonds and the general skeletal geometry of the cluster. The solution dynamics of **6** as studied by variable-temperature (VT) ^1H and ^{13}C NMR spectroscopies are also reported for comparison with the analogous complex $[(\mu_3\text{-}\eta^2\text{-}C_2\text{-}t\text{-}Bu)(CO)_9Ru_3]_2(\mu_4\text{-}Hg)$ (**5**). Compound **1** crystallizes in the triclinic space group $P\bar{1}$ with a = 9.339 (1) Å, b = 10.773 (2) Å, c = 14.666 (4) Å, α = 96.00 (2)°, β = 108.00 (2)°, γ = 91.70 (1)°, V = 1393 (2) Å^3, and Z = 2. Least-squares refinement of 3726 observed reflections gave a final R = 0.045 (R_w = 0.051). Compound **2** crystallizes in the triclinic space group $P\bar{1}$ with a = 10.710 (1) Å, b = 14.639 (3) Å, c = 9.310 (3) Å, α = 107.90 (2)°, β = 92.65 (2)°, γ = 96.02 (1)°, V = 1377 (2) Å^3, and Z = 2. Least-squares refinement of 3535 observed reflections gave a final R = 0.045 (R_w = 0.053). Compound **3** crystallizes in the monoclinic space group $P2_1/n$ with a = 15.890 (4) Å, b = 12.629 (3) Å, c = 15.299 (3) Å, β = 104.16 (2)°, V = 2977 (2) Å^3, and Z = 4. Least-squares refinement of 3301 observed reflections gave a final R = 0.067 (R_w = 0.072). Compound **4** crystallizes in the orthorhombic space group *Pbca* with a = 16.574 (5) Å, b = 18.251 (5) Å, c = 18.445 (5) Å, V = 5580 (3) Å^3, and Z = 8. Least-squares refinement of 2814 observed reflections gave a final R = 0.049 (R_w = 0.053). Compound **6** crystallizes in the triclinic space group $P\bar{1}$ with a = 9.363 (3) Å b = 20.814 (3) Å, c = 9.030 (2) Å, α = 91.61 (1)°, β = 115.82 (2)°, γ = 95.51 (2)°, V = 1572 (1) Å^3, and Z = 2. Least-squares refinement of 3896 observed reflections gave a final R = 0.077 (R_w = 0.082).

Introduction

We have been studying the chemistry of mercury-bridged transition-metal clusters of the general type $(\mu_3\text{-L})M_3(\mu_3\text{-Hg})M'$ and $[(\mu_3\text{-L})M_3]_2(\mu_4\text{-Hg})$ where μ_3-L = capping ligand, M = Ru or Os, and M′ = mononuclear transition-metal moiety (see Figure 1), with the goals of establishing relative reactivity patterns for different types of mercury–transition-metal bonds and developing new routes to mixed-transition-metal clusters by thermally or photochemically induced reductive elimination of mercury.[1-3] Since our initial reports, other workers have reported similar types of mercury-bridged trinuclear clusters with different transition metals,[4-9] several of which contain face capping[5,6,9] as well as edge bridging mercury atoms.[4,7,8]

The structural features of the $(\mu_3\text{-L})M_3(\mu_3\text{-Hg})M'$ class of molecules are interesting for several reasons. First, they represent a relatively rare coordination number (three) for mercury, and it would be interesting to observe deviations from the expected planar arrangement of the transition-metal atoms as a function of their ancillary ligands and the geometry around M′. Second, these molecules contain both normal 2-center–2-electron and electron-deficient 3-center–2-electron mercury–transition-metal bonds, and it would be instructive to observe how μ-Hg bonding parameters such as the M′–Hg bond length, the M–M edge distances, and the M_3Hg butterfly angles vary with substitution of different M's in the $(\mu_3\text{-L})M_3(\mu_3\text{-Hg})M'$ system. Our reactivity studies on this class of molecules required the synthesis of a broad range of complexes, and in light of this, we thought it would be informative to undertake solid-state structural investigations on a homologous series of these complexes.

We report here the synthesis and solid-state structures of $(\mu_3\text{-}\eta^2\text{-}C_2\text{-}t\text{-}Bu)(CO)_9Ru_3(\mu_3\text{-}Hg)Ru(\eta^5\text{-}C_5H_5)(CO)_2$ (**1**), $(\mu_3\text{-}\eta^2\text{-}C_2\text{-}t\text{-}Bu)(CO)_9Ru_3(\mu_3\text{-}Hg)Fe(\eta^5\text{-}C_5H_5)(CO)_2$ (**2**), $(\mu_3\text{-}\eta^2\text{-}C_2\text{-}t\text{-}Bu)(CO)_9Os_3(\mu_3\text{-}Hg)Mo(\eta^5\text{-}C_5H_5)(CO)_3$ (**3**), and $(\mu_3\text{-}\eta^2\text{-}C_2\text{-}t\text{-}Bu)(CO)_9Os_3(\mu_3\text{-}Hg)Co(CO)_4$ (**4**). The choice of compounds for structural studies presented here was dictated by the availability of suitable crystals for X-ray diffraction examination rather than by any synthetic limitation.

We have also been studying the related μ_4-mercury complex $[(\mu_3\text{-}\eta^2\text{-}C_2\text{-}t\text{-}Bu)(CO)_9Ru_3]_2(\mu_4\text{-}Hg)$ (**5**) (Figure 1) where the geometry around mercury is intermediate between square planar and tetrahedral (i.e., the angle between the two $Ru_2(\mu_3\text{-}Hg)$ planes is 44.5°).[2] This compound is skeletally chiral and exhibits unique dynamical properties in solution as monitored by VT-^1H and ^{13}C NMR spectroscopies (vida infra). We have now extended the synthesis of this type of chiral cluster to the osmium

† For parts 1–4, see refs 1–3 and 18.

‡ Present address: Departimento Chimica Inorganica, Fisicia ed Materiale, Universitā di Torino, Turin, Italy.

(1) Rosenberg, E.; King, K.; Fahmy, R.; Tiripicchio, A. *J. Am. Chem. Soc.* **1980**, *102*, 3626.
(2) Rosenberg, E.; Hardcastle, K. I.; Ermer, S.; King, K.; Tiripicchio, A. *Inorg. Chem.* **1983**, *22*, 1339.
(3) Rosenberg, E.; Wang, J.; Gellert, R. G. *Organometallics* **1988**, *7*, 1093.
(4) Duffy, D. N.; Mackay, K.; Nicholson, B. *J. Chem. Soc., Dalton Trans.* **1981**, 381.
(5) Braunstein, P.; Tiripicchio, A.; Rose, J.; Tiripicchio-Camellini, M. *J. Chem. Soc., Chem. Commun.* **1984**, 391.
(6) Venanzi, L.; Albinati, M.; Moor, A.; Pregosin, P. S. *J. Am. Chem. Soc.* **1982**, ^{0}4, 7672.
(7) Mays, M. J.; Iggo, J. A. *J. Chem. Soc., Dalton Trans.* **1984**, 644.
(8) Farrugia, L. J. *J. Chem. Soc., Chem. Commun.* **1987**, 147.
(9) Wang, J.; Sabat, M.; Horwitz, C. P.; Shriver, D. F. *Inorg. Chem.* **1988**, *27*, 552.

0276-7333/91/2310-0203$02.50/0

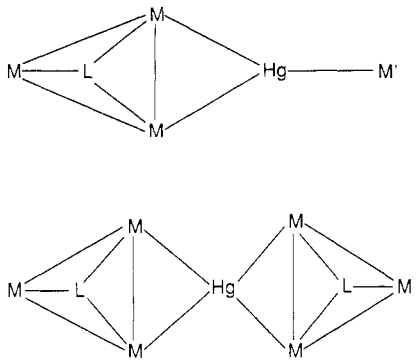

Figure 1. Structural types of mercury-bridged metal clusters.

sulfur capped analogue $[(\mu\text{-H})(\mu_3\text{-S})(CO)_9Os_3]_2(\mu_4\text{-Hg})$ (**6**). We report here the solid-state structure of **6** along with its VT-^{1}H and ^{13}C NMR spectral data for comparison with **5**.

Results and Discussion

A. Synthesis of Compounds 1–4 and 6. Synthesis of the ruthenium-based mixed-transition-metal complexes **1** and **2** can be accomplished by the route represented in eq 1. Synthesis of the hydride complex and subsequent

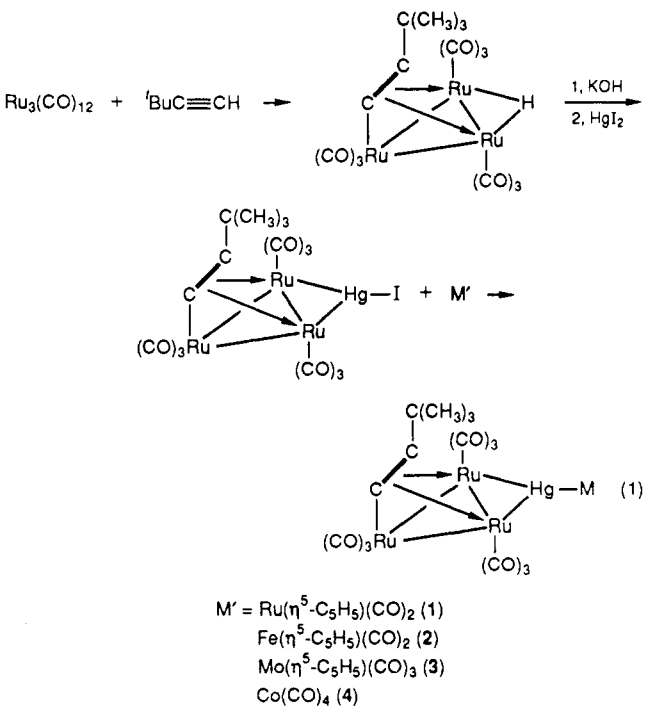

$M' = Ru(\eta^5\text{-}C_5H_5)(CO)_2$ (**1**)
$Fe(\eta^5\text{-}C_5H_5)(CO)_2$ (**2**)
$Mo(\eta^5\text{-}C_5H_5)(CO)_3$ (**3**)
$Co(CO)_4$ (**4**)

deprotonation proceeds almost quantitatively from ruthenium carbonyl with overall conversion to the iodomercurial cluster in about 60–70% yield. Compounds **1** and **2** are obtained in poor to moderate yields, 20–30%, with the chief byproduct being **5**. Apparently, formation of **5** from the corresponding iodide is promoted by addition of the electron-rich carbonyl metallates. This problem is particularly severe in the synthesis of **2** where ~40% **5** is observed along with 20% **2**. Formation of **5** would be expected to be accompanied by the formation of $Hg[M(\mu^5\text{-}C_5H_5)(CO)_2]_2$ (M = Fe, Ru) according to the expected redistribution reaction (eq 2).

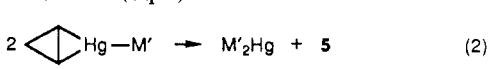

The latter compounds are quite insoluble, however, and are obscured in the reaction residues by decomposition byproducts and the salts produced in the metathesis reaction. Methylene chloride extracts of the reaction residues did give infrared spectra consistent with the presence of these compounds, but it was not possible to quantify their amounts.

The synthesis of **3** and **4** proceeds by the same overall route except for the synthesis of the starting hydride (eq 3). Direct reaction of $Os_3(CO)_{12}$ with *tert*-butylacetylene

$$Os_3(CO)_{12} + CH_3CN \xrightarrow[Me_3NO]{} Os_3(CO)_{10}(CH_3CN)_2 \xrightarrow{{}^tBuC{\equiv}CH} ({}^tBuC{\equiv}CH)Os_3(CO)_{10} \rightarrow (\mu\text{-H})(\mu_3\text{-}\eta^5\text{-}C_2{}^tBu)Os_3(CO)_9 \quad (3)$$

yields a complex mixture of products containing only a small amount (5–10%) of the desired hydride product, so the well-known route via $(Os_3(CO)_{10}(CH_3CN)_2$ was utilized.[10] Subsequent conversion to the mercurial iodide and then to **3** and **4** proceeds in moderate yield (~60% based on $Os_3(CO)_{12}$). Interestly, little or no formation of the osmium analogue of **5** is noted. Thus, the apparent redistribution reactions (eq 2) probably proceed more slowly in the case of **3** and **4** compared to their ruthenium analogues.

The synthesis of **6** is accomplished by the overall process outlined in eq 4. Deprotonation of $(\mu_3\text{-S})(\mu\text{-H})_2Os_3(CO)_9$[11,12] is best performed by using potassium hydroxide

$$Os_3(CO)_{12} \xrightarrow[H_2S]{} (\mu\text{-H})_2Os_3(\mu_3\text{-S})(CO)_9 \xrightarrow[KH]{KOH\ or} (\mu\text{-H})Os_3(\mu_3\text{-S})(CO)_9^- \xrightarrow[HgI_2]{} [(\mu\text{-H})Os_3(\mu_3\text{-S})(CO)_9]_2(\mu_4\text{-Hg}) \quad (4)$$

or potassium hydride with subsequent conversion to **6** proceeding in good yield. It is interesting to note that we were able to prepare the unsymmetrical mercurial complex $(\mu_3\text{-S})(CO)_9Os_3(\mu\text{-Hg})I$ by this route by simply using an excess of mercury(II) iodide. However, this compound proved to be very unstable in solution with respect to the formation of **6** and presumably HgI_2.[13] It can be concluded from these observations that the efficiency with which the redistribution reactions (eq 2) occur is not only dependent on the nature of metal atoms in the trinuclear cluster but also on the nature of the capping ligand.

B. Solid-State Structures of Compounds 1–4. The solid-state structures of compounds **1–4** are shown in Figures 2–5. Crystal data for compounds **1–4** are given in Table I. Selected bond distances and angles are given in Tables II–V. All of these compounds are structurally related by having a three-coordinate mercury atom. The Hg–M′ distances for the 2-center–2-electron bonds fall within the expected ranges for these bonds in related complexes. Thus, the Hg–Fe distance in **2** of 2.512 (2) Å is in between that found for the same distance in $Hg[Fe(CO)_2NOP(CH_2CH_3)_3]_2$ (2.534 (2) Å)[14] and $[(\eta^5\text{-}C_5H_5)(CO)_2FeHgCo(CO)_4]$ (2.49 Å).[15] It appears from these results that the ancillary ligands bound to the iron and the nature of the other group bound to mercury have little effect on the length of the 2-center–2-electron Hg–Fe bond. Similarly, the Hg–Mo bond in **3** (2.718 (3) Å) is only

(10) Deeming, A. J.; Aime, S. *J. Chem. Soc., Dalton Trans.* **1983**, 1807.
(11) Forster, A.; Johnson, B. F. G.; Lewis, J.; Matheson, T. W. *J. Organomet. Chem.* **1976**, *104*, 225.
(12) Johnson, B. F. G.; Lewis, J.; Pippard, P. A. *J. Organomet. Chem.* **1981**, *213*, 249.
(13) Rosenberg, E.; Hajela, S.; Petrik, P. Unpublished results.
(14) Stephens, F. S. *J. Chem. Soc., Dalton Trans.* **1972**, 2257.
(15) Bryan, R. F.; Welser, P. *Acta Crystallogr.* **1966**, *A21*, 138.

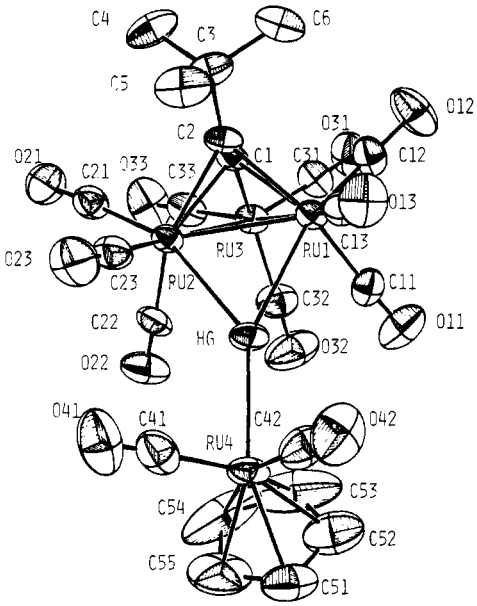

Figure 2. ORTEP drawing of compound **1**.

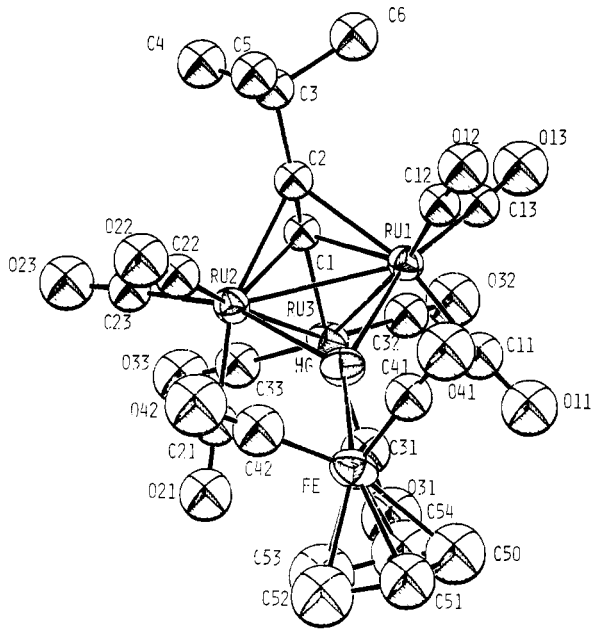

Figure 3. ORTEP drawing of compound **2**.

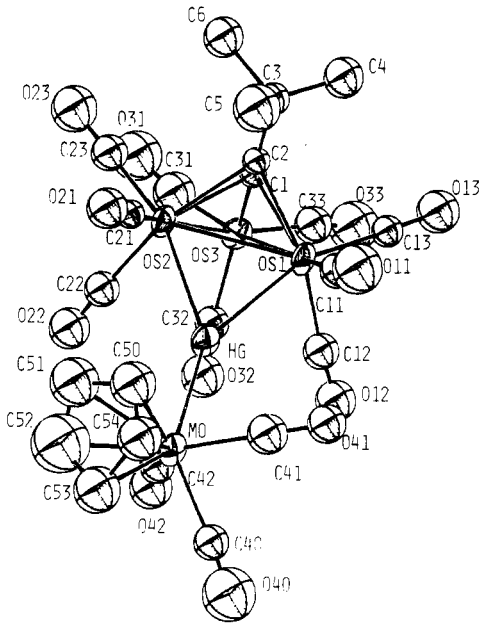

Figure 4. ORTEP drawing of compound **3**.

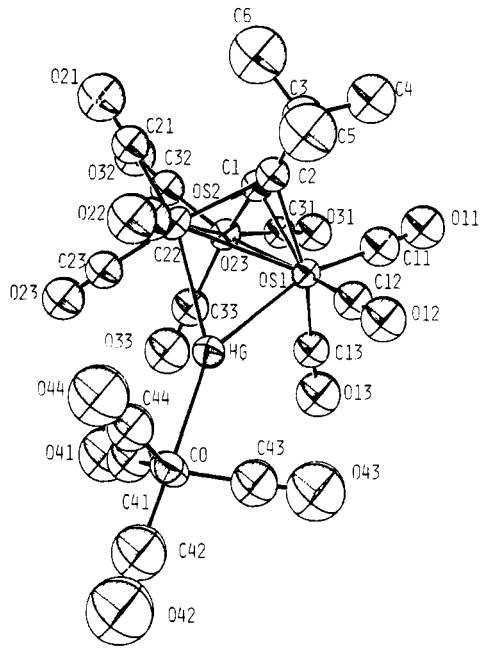

Figure 5. ORTEP drawing of compound **4**.

slightly shorter than that found in $Hg[Mo(\eta^5\text{-}C_5H_5)(CO)_3]_2$ (2.746 (2) Å),[16] and the Hg–Co bond in **4** (2.514 (4) Å) is only slightly longer than that found in $Hg[Co(CO)_4]_2$ systems (2.50 Å).[5,17] It is interesting to note that the Hg–Ru bond in **1** is significantly shorter (2.602 (1) Å) than the corresponding bond in the related complex *cis*-$[(\mu_3\text{-}\eta^2\text{-}C_2\text{-}t\text{-}Bu)(CO)_9Ru_3(\mu_3\text{-}Hg)]_2Ru(CO)_4$ (2.658 (1) Å).[18] In the latter complex, a Hg–Hg bonding interaction was suggested based on the *cis*-Hg–Ru–Hg angle (84°). This same trend is observed in the iron complexes *cis*-$Fe(CO)_4(HgBr)_2$[19] and **2** where the Fe–Hg bond lengths are 2.59 and 2.512 (3) Å, respectively, and where the *cis*-Hg–Fe–Hg angle is 81°. Thus, Hg–Hg bonding in the *cis*-Hg_2M (M = Fe, Ru) complexes causes elongation in the 2-center-2-electron Hg–Ru bond, and the shorter value observed in **1** (2.602 (1) Å) should be taken as the more typical value for this previously unreported bond length.

The 3-center-2-electron μ-Hg–M_2 (M = Ru, Os) bonds in complexes **1–3** fall within a remarkably narrow range (2.826–2.837 Å). The direct ruthenium analogue of **3**, $(\mu_3\text{-}\eta^2\text{-}C_2\text{-}t\text{-}Bu)(CO)_9Ru_9(\mu_3\text{-}Hg)Mo(\eta^5\text{-}C_5H_5)(CO)_3$ shows only a slightly shorter μ-Hg–M distance of 2.812 (2) Å.[2] Although it is not unusual for Ru–Ru and Os–Os distances to be very similar in similar metal clusters, it is rare to find such correspondence in Ru and Os bonds to a different element (i.e., Hg).[20] This point is further illustrated by the fact that the Os–Os bonds at the unbridged edges in **3** are significantly (0.04–0.05 Å) longer than the analogous bonds in **2** and in $(\mu_3\text{-}\eta^2\text{-}C_2\text{-}t\text{-}Bu)(CO)_9Ru_3(\mu_3\text{-}Hg)Mo(\eta^5\text{-}C_5H_5)(CO)_3$. Compound **4** is distinctly different from

(16) Mickiewicz, M. M.; Raston, C. L.; White, A. A.; Wild, S. B. *Aust. J. Chem.* **1977**, *30*, 1685.
(17) Sheldrick, G. M.; Simpson, R. N. F. *J. Chem. Soc. A* **1968**, 1005.
(18) Rosenberg, E.; Ryckman, D.; Hsu, I.; Gellert, R. W. *Inorg. Chem.* **1968**, *25*, 194.
(19) Dahl, L. F.; Baird, H. W. *J. Organomet. Chem.* **1967**, *7*, 503.
(20) Johnson, B. F. G. *Transition Metal Clusters*; John Wiley & Sons: New York, 1980; p 471.

Table I. Summary of Crystal and Intensity Data

	compound 1	compound 2	compound 3	compound 4	compound 6
formula	$C_{22}H_{14}O_{11}Ru_4Hg$	$C_{22}H_{14}O_{11}FeRu_3Hg$	$C_{23}H_{14}O_{12}MoOs_3Hg$	$C_{19}H_9O_{13}CoOs_3Hg$	$C_{18}H_2O_{18}S_2Os_6Hg$
fw, amu	1059.22	1013.93	1349.49	1275.40	1912.12
system	triclinic	triclinic	monoclinic	orthorhombic	triclinic
a, Å	9.339 (1)	10.710 (1)	15.890 (4)	16.574 (5)	9.363 (3)
b, Å	10.773 (2)	14.639 (3)	12.629 (3)	18.251 (5)	20.814 (3)
c, Å	14.666 (4)	9.310 (3)	15.299 (3)	18.445 (5)	9.030 (2)
α, deg	96.00 (2)	107.90 (2)	90.00 (2)	90.00 (2)	91.61 (1)
β, deg	108.00 (2)	92.65 (2)	104.16 (2)	90.00 (2)	115.82 (2)
γ, deg	91.70 (1)	96.02 (1)	90.00 (2)	90.00 (2)	95.51 (2)
V, Å^3	1393 (2)	1377 (2)	2977 (2)	5580 (2)	1572 (1)
space group	$P\bar{1}$ (No. 2)	$P\bar{1}$ (No. 2)	$P2_1/n$	$Pbca$ (No. 61)	$P\bar{1}$ (No. 2)
Z	2	2	4	8	2
ρ(calc), g cm^{-3}	2.53	2.45	3.01	3.04	4.04
μ, cm^{-1} (Mo Kα)	76.3	77.2	183.3	197.5	292.6
crystal size, mm^3	0.15 × 0.15 × 0.20	0.10 × 0.20 × 0.20	0.38 × 0.42 × 0.15	0.20 × 0.20 × 0.50	0.03 × 0.12 × 0.16
λ(Mo Kα), Å (graphite monochromator)	0.71073	*a*	*a*	*a*	*a*
temp for data collecn, °C	25 (1)	*a*	*a*	*a*	*a*
systematic absences	none	none	$h0l$, $h + l = 2n + 1$ $0k0$, $k = 2n + 1$	$hk0$, $h = 2n + 1$ $h0l$, $l = 2n + 1$ $0kl$, $k = 2n + 1$	none
rel transmissn coeff range (ψ scans)	0.621–0.998	0.641–0.998	0.664–0.997	0.462–0.998	0.421–0.987
θ range, data collecn	1–25.0	1–25.0	1–25.0	1–27.0	1–25.0
structure soln method	Patterson	Patterson	direct methods	direct methods	direct methods
unique data measd	4890	4825	5706	5505	5516
obs data with $\lvert F_o\rvert > 3\sigma(F_o)$	3726	3535	3301	2814	3896
no. of variables	344	179	187	175	226
R[b]	0.045	0.045	0.067	0.049	0.077
R_1[c]	0.051	0.053	0.072	0.053	0.082
weighting scheme, w	$4(F_o)^2/[\sigma(F_o)^2]^2$	*a*	*a*	*a*	*a*
highest residual in final ΔF map, e Å^{-3}	2.74 (22)	1.10 (22)	2.04 (28)	1.24 (24)	2.65 (68)
largest shift/esd	0.01	0.02	0.26	0.13	0.00

[a] Same entry as for compound 1. [b] $R = \sum(\lvert F_o\rvert - \lvert F_c\rvert)/\sum\lvert F_o\rvert$. [c] $R_w = [\sum w(\lvert F_o\rvert - \lvert F_c\rvert)^2/\sum w(F_o)^2]^{1/2}$.

Table II. Bond Distances (Å) and Angles (deg) for $(\mu_3$-η^2-C_2-*t*-Bu)$(CO)_9Ru_3(\mu_3$-Hg)Ru$(\eta^5$-$C_5H_5)(CO)_2$ (1)[a]

Distances			
Hg–Ru1	2.826 (1)	Ru3–C1	1.96 (1)
Hg–Ru2	2.834 (1)	C1–C2	1.28 (1)
Hg–Ru4	2.602 (1)	C2–C3	1.55 (1)
Ru1–Ru2	2.853 (1)	C3–C4	1.55 (1)
Ru1–Ru3	2.805 (1)	C3–C5	1.54 (1)
Ru1–C1	2.20 (1)	C3–C6	1.53 (1)
Ru1–C2	2.23 (1)	Ru–C(Cp)	2.23 (1)*
Ru2–Ru3	2.800 (1)	Ru–C(CO)	1.86 (1)*
Ru2–C1	2.18 (1)	C–O(CO)	1.13 (1)*
Ru2–C2	2.26 (1)	C–C(Cp)	1.40 (3)*
Angles			
Ru1–Hg–Ru2	60.52 (2)	Ru2–Ru1–Ru3	59.32 (2)
Ru1–Hg–Ru4	154.92 (3)	Ru1–Ru2–Ru3	59.50 (2)
Ru2–Hg–Ru4	143.00 (2)	Hg–Ru2–Ru3	99.61 (2)
Hg–Ru1–Ru2	59.87 (2)	Ru1–Ru3–Ru2	61.18 (2)
Hg–Ru1–Ru3	99.67 (2)	M–C–O	177 (1)*
Hg–Ru2–Ru1	59.61 (2)		

[a] Numbers in parentheses are estimated standard deviations in the least significant digits. * = average values.

Table III. Bond Distances (Å) and Angles (deg) for $(\mu_3$-η^2-C_2-*t*-Bu)$(CO)_9Ru_3(\mu_3$-Hg)Fe$(\eta^5$-$C_5H_5)(CO)_2$ (2)[a]

Distances			
Hg–Ru1	2.833 (1)	Ru3–C1	1.95 (1)
Hg–Ru2	2.837 (1)	C1–C2	1.30 (2)
Hg–Fe	2.512 (3)	C2–C3	1.52 (2)
Ru1–Ru2	2.854 (1)	C3–C4	1.53 (2)
Ru1–Ru3	2.803 (1)	C3–C5	1.54 (2)
Ru1–C1	2.19 (1)	C3–C6	1.56 (2)
Ru1–C2	2.25 (1)	Fe–C(Cp)	2.11 (2)*
Ru2–Ru3	2.800 (2)	Fe–C(CO)	1.72 (2)*
Ru2–C1	2.17 (1)	Ru–C(CO)	1.88 (2)*
Ru2–C2	2.27 (1)	C–O(CO)	1.15 (2)*
		C–C(Cp)	1.42 (4)*
Angles			
Ru1–Hg–Ru2	60.43 (3)	Ru1–Ru3–Ru2	61.23 (4)
Ru1–Hg–Fe	155.14 (6)	Ru2–Ru1–Ru3	59.32 (4)
Ru2–Hg–Fe	143.08 (6)	Ru1–Ru2–Ru3	59.45 (4)
Hg–Ru1–Ru2	59.86 (3)	Hg–Ru2–Ru3	99.37 (4)
Hg–Ru1–Ru3	99.39 (4)	M–C–O	177 (1)*
Hg–Ru2–Ru1	59.71 (3)		

[a] Numbers in parentheses are estimated standard deviations in the least significant digits. * = average values.

1–3 in that its μ-Hg–Os bonds are significantly shorter (2.775 (1) and 2.774 (1) Å). This shortening of μ-Hg–Os bonds in 4 is accompanied by a significant lengthening of the Os–Os bond length at the mercury-bridged edge of the Os_3 triangle (2.917 (1) Å in 4 and 2.853 (1) to 2.876 (2) Å in 1–3). These bond lengths in 4 are very similar to those found in $(\mu_3$-η^2-C_2-*t*-Bu$)(CO)_9Ru_3(\mu$-Hg)Br where the μ-Hg–Ru distances are 2.733 (2) and 2.739 (2) Å and the Ru–Ru distance at the mercury-bridged edge is 2.900 (3) Å.[1] We suggest here that the significant differences in these bonds between 1–3 and 4 and the similarity between 4 and $(\mu_3$-η^2-C_2-*t*-Bu$)(CO)_9Ru_3(\mu$-Hg)Br is due to the expected greater electronegativity of the $Co(CO)_4^-$ moiety compared with Fe$(\eta^5$-$C_5H_5)(CO)_2^-$ and Mo$(\eta^5$-$C_5H_5)(CO)_3^-$. This is supported by the fact that $HCo(CO)_4$ is a much stronger acid than either HMo$(\eta^5$-$C_5H_5)(CO)_3$ or HFe-$(\eta^5$-$C_5H_5)(CO)_2$.[21]

The shortening of Os–Hg bonds in 4 is accompanied by two other structural changes that set it apart from 1–3. First, the displacement of the mercury atom above the Os(1)–Os(2)–Co plane is (see Figure 1) +0.09 Å in 4 and −0.14, −0.16, and +0.04 Å in 1, 2, and 3, respectively. Second, the M_3–Hg butterfly angles are 125, 124, and 126°

(21) Collman, J. P.; Hegedus, L. S.; Norton, J. R.; Finke, R. G. *Principles and Applications in Organotransition Metal Chem.*; University Science Books: Mill Valley, CA, 1987; pp 91–84.

Table IV. Bond Distances (Å) and Angles (deg) for $(\mu_3\text{-}\eta^2\text{-}C_2\text{-}t\text{-}Bu)(CO)_9Os_3(\mu_3\text{-}Hg)Mo(\eta^5\text{-}C_5H_5)(CO)_3$ (3)[a]

Distances			
Hg–Os1	2.826 (2)	Os3–C1	1.93 (3)
Hg–Os2	2.833 (2)	C1–C2	1.29 (4)
Hg–Mo	2.718 (3)	C2–C3	1.54 (4)
Os1–Os2	2.876 (2)	C3–C4	1.51 (6)
Os1–Os3	2.830 (2)	C3–C5	1.49 (6)
Os1–C1	2.20 (3)	C3–C6	1.58 (6)
Os1–C2	2.18 (3)	Mo–C(Cp)	2.30 (6)*
Os2–Os3	2.840 (2)	Mo–C(CO)	1.96 (4)*
Os2–C1	2.19 (3)	C–O(CO)	1.13 (5)*
Os2–C2	2.20 (3)	C–C(Cp)	1.32 (8)*
		Os–C(CO)	1.89 (4)*
Angles			
Os1–Hg–Os2	61.09 (5)	Hg–Os2–Os1	59.34 (5)
Os1–Hg–Mo	150.72 (8)	Hg–Os2–Os3	100.05 (7)
Os2–Hg–Mo	148.13 (9)	Os1–Os2–Os3	59.37 (5)
Hg–Os1–Os2	59.56 (5)	Os1–Os3–Os2	60.96 (4)
Hg–Os1–Os3	100.43 (5)	M–C–O	174 (4)*
Os2–Os1–Os3	59.67 (5)		

[a] Numbers in parentheses are estimated standard deviations in the least significant digits. * = average values.

Table V. Bond Distances (Å) and Angles (deg) for $(\mu_3\text{-}\eta^2\text{-}C_2\text{-}t\text{-}Bu)(CO)_9Os_3(\mu_3\text{-}Hg)Co(CO)_4$ (4)[a]

Distances			
Hg–Os1	2.775 (1)	Os3–C1	1.90 (2)
Hg–Os2	2.774 (1)	C1–C2	1.29 (3)
Hg–Co	2.514 (4)	C2–C3	1.59 (4)
Os1–Os2	2.917 (1)	C3–C4	1.51 (5)
Os1–Os3	2.848 (1)	C3–C5	1.44 (5)
Os1–C1	2.21 (2)	C3–C6	1.53 (6)
Os1–C2	2.21 (3)	Co–C(CO)	1.74 (4)*
Os2–Os3	2.829 (1)	Os–C(CO)	1.88 (3)*
Os2–C1	2.20 (2)	C–C(CO)	1.17 (4)*
Os2–C2	2.21 (3)		
Angles			
Os1–Hg–Os2	63.43 (4)	Hg–Os2–Os1	58.30 (3)
Os1–Hg–Co	148.6 (2)	Hg–Os2–Os3	93.72 (5)
Os2–Hg–Co	147.5 (2)	Os1–Os2–Os3	59.40 (3)
Hg–Os1–Os2	58.27 (4)	Os1–Os3–Os2	61.83 (4)
Hg–Os1–Os3	93.29 (5)	M–C–O	176 (3)*
Os2–Os1–Os3	58.77 (3)		

[a] Numbers in parentheses are estimated standard deviations in the least significant digits. * = average values.

in **1**, **2**, and **3**, respectively, while it is 117° in **4**. These structural changes can also be rationalized on the basis of the greater electronegativity of the $Co(CO)_4^-$ moiety. The more electronegative the M′ group bound to mercury, the more the low-lying empty p–d orbitals on mercury would be expected to be involved in bonding. This would lead to a more tetrahedral-like configuration around mercury and a requisite closing of its geometry. This electronegativity effect on the geometry around the mercury atom in **4** is also seen in $(\mu_3\text{-}\eta^2\text{-}C_2\text{-}t\text{-}Bu)(CO)_9Ru_3(\mu\text{-}Hg)Br$, which forms a bromine-bridged dimer in the solid state in which the mercury atom is in a distorted tetrahedral environment.[1] These observations lead us to conclude that the most important factors in determining the geometry and bond lengths around mercury in **1**–**4** are the electronic properties of M′. If steric factors were an important consideration, one would expect the μ-Hg–M bonds and the butterfly angles in **1**, **2**, and **3** to be more different from each other than they are.

Solid-State Structure and VT-^{13}C NMR of 6. The solid-state structure of **6** is illustrated in Figure 6. Crystal data for compound **6** are given in Table I. Selected bond distances and angles are given in Table VI. The overall geometry of the compound is very similar to **5**, with the geometry around mercury being a slightly flattened tetrahedron.[2] As in **5**, the molecule possesses a C_2 axis (perpendicular to the plane of the paper in Figure 6) but is chiral by virtue of the screw axis bisecting the mercury-bridged Os–Os edges and passing through the mercury atom. The dihedral angle between the Hg–Os(1)–Os(2) plane and the Hg–Os(4)–Os(5) plane is 65°, significantly different from the analogous angle in **5** (44.5°).

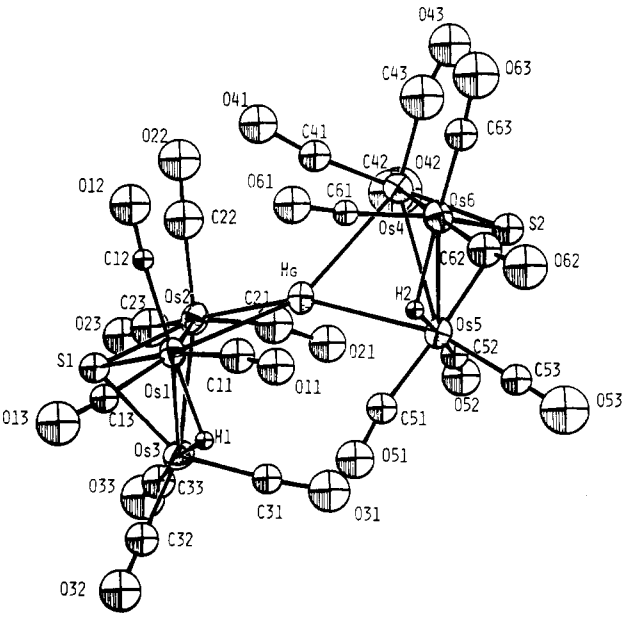

Figure 6. ORTEP drawing of compound **6**.

Table VI. Bond Distances (Å) and Angles (deg) for $[(\mu\text{-}H)(\mu_3\text{-}S)(CO)_9Os_3]_2(\mu_4\text{-}Hg)$ (6)[a]

Distances			
Hg–Os1	2.834 (2)	Os3–S1	2.37 (1)
Hg–Os2	2.815 (2)	Os4–Os5	2.985 (2)
Hg–Os4	2.817 (2)	Os4–Os6	2.758 (2)
Hg–Os5	2.830 (2)	Os4–S2	2.37 (1)
Os1–Os2	2.978 (2)	Os5–S2	2.40 (1)
Os1–Os3	2.920 (2)	Os5–Os6	2.917 (2)
Os1–S1	2.38 (1)	Os6–S2	2.36 (1)
Os2–Os3	2.756 (2)	Os–C(CO)	1.89 (4)*
Os2–S1	2.36 (1)	Os–H	1.85*
		C–O(CO)	1.14 (5)*
Angles			
Os1–Hg–Os2	63.64 (6)	Hg–Os2–Os1	58.50 (6)
Os1–Hg–Os4	146.87 (6)	Os1–Os3–Os2	63.23 (4)
Os1–Hg–Os5	128.37 (8)	Hg–Os4–Os5	58.31 (4)
Os2–Hg–Os4	126.90 (7)	Hg–Os4–Os6	93.13 (6)
Os2–Hg–Os5	145.70 (7)	Os5–Os4–Os6	60.89 (5)
Os4–Hg–Os5	63.82 (5)	Os4–Os5–Os6	55.71 (5)
Hg–Os1–Os2	57.86 (6)	Hg–Os5–Os4	57.87 (4)
Hg–Os1–Os3	88.36 (5)	Hg–Os5–Os6	89.56 (5)
Os2–Os1–Os3	55.70 (4)	Os4–Os6–Os5	63.40 (5)
Os1–Os2–Os3	61.07 (6)	Os–C–O	174 (4)*
Hg–Os2–Os3	92.09 (6)		

[a] Numbers in parentheses are estimated standard deviations in the least significant digits. * = average values.

The μ-Hg–Os bond lengths are virtually identical with those in complexes **1**–**3** with an average value of 2.82 Å. The Os–Os vectors on the mercury-bridged edges are considerably elongated (Os(1)–Os(2) = 2.978 (2) Å, Os(4)–Os(5) = 2.985 (2) Å) compared with those in **1**–**3** and are significantly longer than those in **4** and **5** (2.85 Å).[2] Interestingly, the mercury-bridged osmium edges are significantly longer than the hydride-bridged edges (Os(1)–Os(3) = 2.920 (2) Å, Os(5)–Os(6) = 2.917 (2) Å), suggesting more removal of metal–metal bond electron density by mercury than by hydrogen. This weakening of the osmium–osmium interaction at the hydride- and mercury-

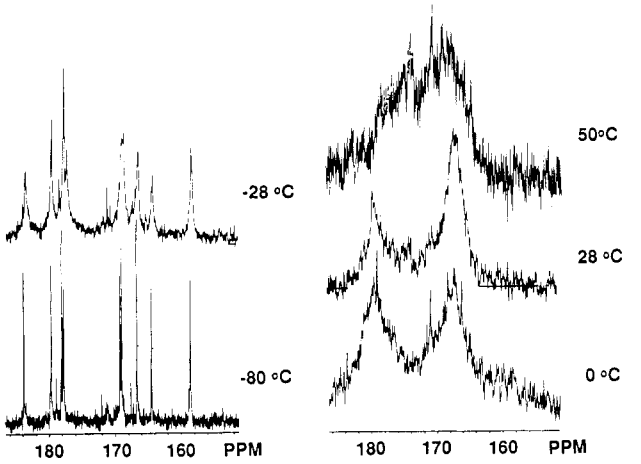

Figure 7. VT-^{13}C NMR spectra of compound **6** at 68 MHz in CD_2Cl_2.

bridged edges is apparently compensated for by a stronger Os–Os interaction at the unbridged edges of each Os_3 unit which have very short Os–Os distances (Os(2)–Os(3) = 2.756 (2) Å and Os(4)–Os(6) = 2.758 (2) Å). The Os–S bonds to the capping ligand are all essentially the same and are similar to those found in $H_2Os_3(CO)_9S$.[11] The hydride ligands in **5** were located by using the program HYDEX,[22] and they have a cisoid relationship to each other (Figure 6) and are located below the plane of each Os_3 triangle opposite the sulfur-capped face. The butterfly angles of the two Os_3Hg wings (114 and 112°) are similar to those found in **5**.

The VT-^{1}H NMR spectrum of **6** at 400 MHz shows a low-temperature limiting spectrum at −93 °C consisting of two hydride resonances at −22.43 and −20.98 ppm in a relative intensity ratio of 1.0 to 0.04. This points to the existence of two isomers in solution. Above −50 °C, the low-intensity hydride signal is broadened into the base line. Between −50 and +22 °C, we observe a steady downfield shift and progressive sharpening of the major hydride resonance which appears at −22.26 ppm at +22 °C, reflecting the increasing population of the minor isomer. Using the low-temperature limiting spectrum chemical shifts and correcting for the expected changes in population (assuming $\Delta S \cong 0$), we calculated a chemical shift of −22.24 ppm at +22 °C in reasonable agreement with the observed value. A reasonable assignment for the minor isomer is a structure in which the two hydrides are in a transoid relationship to each other. This minor isomer also possesses a C_2 axis (making both hydrides equivalent within each isomer) but rotated (~30°) with respect to the C_2 axis in the major cisoid isomer as one looks down the sulfur–sulfur vector.

The low-temperature limiting VT-^{13}C NMR of **6** at 68 MHz in the carbonyl region is observed at −80 °C in THF-d_8 and shows nine resonances of approximately equal intensity at 183.6, 179.6, 177.9, 177.6, 169.1, 168.8, 166.5, 164.3, and 158.3 ppm (Figure 7). Four low-intensity peaks at 178.7, 171.9, 167.4, and 158.6 ppm are also observed at this temperature, which are attributed to a minor impurity since the lines do not broaden with the major peaks. At −28 °C, all resonances show appreciable broadening, and by +28 °C, the resonances have averaged into two broadened resonances at 167.2 and 179.8 ppm in a ratio of approximately 2:1. At +50 °C, these resonances broaden further and appear to be averaging with each other. This dynamic behavior closely parallels the two-stage-exchange process observed for $(\mu\text{-H})_2Os_3(CO)_9(\mu_3\text{-S})$ where hydride motion averages all equatorial carbonyls with each other and all axial carbonyls with each other before the onset of axial radial exchange at each osmium atom.[11,23] Motion of both mercury and hydrogen is required to give the observed averaging pattern, as motion of the hydride alone would give nine resonances in the absence of axial–radial carbonyl exchange and three resonances in its presence. It can be concluded from these results that a μ-Hg moiety has about the same mobility on a cluster as a μ-hydride. Similar observations have been made for the related cluster **5** where the mercury atom has about the same mobility as the hydride in its precursor $(\mu\text{-H})Ru_3(CO)_9(\mu_3\text{-}\eta^2\text{-}C_2\text{-}t\text{-Bu})$[24] and for other edge-bridged mercury transition metals compared with their hydride analogues.[8] The greater mobility of the mercury atom in **6** compared with **5** obviously results in racemization of the chiral metal skeleton at much lower temperatures.[24]

Experimental Section

Materials. $Ru_3(CO)_{12}$, $Os_3(CO)_{12}$, $Co_2(CO)_8$, and $[(\eta^5\text{-}C_5H_5)\text{-}Mo(CO)_3]_2$ were purchased from Strem Chemicals and used as received. $(\mu_3\text{-}\eta^2\text{-}C_2\text{-}t\text{-Bu})(CO)_9Ru_3HgI$,[25] $(\mu\text{-H})_2(\mu_3\text{-S})Os_3(CO)_9$,[11] $[(\eta^5\text{-}C_5H_5)Fe(CO)_2]_2$,[26] and $[(\eta^5\text{-}C_5H_5)Ru^2(CO)_2]_2$[27] were synthesized by published literature procedures. Tetrahydrofuran (THF) was distilled from sodium benzophenone ketyl directly before use. Other solvents were stored over type 4a (Linde) molecular sieves. All manipulations, except for thin-layer chromatography (TLC), were conducted under an atmosphere of prepurified nitrogen unless noted otherwise.

Spectra. ^{1}H NMR spectra were obtained on an IBM-NR80 or Bruker-AC 400 NMR spectrometers, and ^{13}C NMR spectra were obtained on a JEOL-270GX instrument. Infrared data were obtained on a Perkin-Elmer 1400 infrared spectrometer.

Synthesis of $(\mu_3\text{-}\eta^2\text{-}C_2\text{-}t\text{-Bu})(CO)_9Ru_3(\mu_3\text{-Hg})Ru(\eta^5\text{-}C_5H_5)(CO)_2$ (1). $[Ru(\eta^5\text{-}C_5H_5)(CO)_2]_2$[27] (500 mg, 1.13 mmol) was dissolved in THF (75 mL). This solution was treated with a 5-fold excess of a 5:1 alloy of K and Na. The reaction proceeded with a gradual color change from orange/amber to purple/brown (overnight). The purple/brown solution was then filtered to yield a 0.03 M solution of $K[Ru(\eta^5\text{-}C_5H_5)(CO)_2]$. Ten milliliters of this solution was slowly added to a cooled (0 °C) solution of $Ru_3(CO)_9(\mu_3\text{-}\eta^2\text{-}C_2\text{-}t\text{-Bu})(\mu\text{-Hg})I$ (300 mg, 0.3 mmol) in THF (65 mL) and stirred for 5 min. The solvent was rotary evaporated and the residue taken up in CH_2Cl_2 and purified by preparative thin-layer chromatography (silica gel with 1:9 CH_2Cl_2:hexanes as eluent). Three bands were eluted, and the middle orange band was collected and recrystallized from hexanes as orange crystals of **1** (180 mg, 0.0170 mmol, 31% yield). IR (CH_2Cl_2) ν(CO): 2082 (w), 2050 (vs), 2007 (s), 1942 (w) cm^{-1}. ^{1}H NMR ($CDCl_3$) δ: 1.39 (9, s), 5.15 (5, s). Anal. Calcd for $C_{22}H_{14}O_{11}Ru_4Hg$: C, 24.94; H, 1.32. Found: C, 24.75; H, 1.45.

Synthesis of $(\mu_3\text{-}\eta^2\text{-}C_2\text{-}t\text{-Bu})(CO)_9Ru_3(\mu_3\text{-Hg})Fe(\eta^5\text{-}C_5H_5)(CO)_2$ (2). $K[Fe(\eta^5\text{-}C_5H_5)(CO)_2]$ (0.6 mmol) was prepared by reduction of $[Fe(\eta^5\text{-}C_5H_5)(CO)_2]_2$ (106 mg, 0.3 mmol) by a 5-fold excess of a 5:1 alloy of K and Na in THF (40 mL). The resulting filtered solution was cooled to −40 °C, and $Ru_3(CO)_9(\mu_3\text{-}\eta^2\text{-}C_2\text{-}t\text{-Bu})(\mu\text{-Hg})I$ (0.578 g, 0.6 mmol) in 20 mL THF was added dropwise with stirring. The solvent was removed in vacuo, and the resulting brown residue was extracted with a minimum amount of CH_2Cl_2 followed by preparative thin-layer chromatography (silica gel with 1:9 CH_2Cl_2:hexanes as eluent). Three bands were eluted. Band 1 (yellow) was identified as **5** by IR spectroscopy in CH_2Cl_2. The middle orange band was collected. Due to its facile interconversion on silica to **5**, **2** was further purified as follows. The main product

(22) Orpen, A. G. *J. Chem. Soc., Dalton Trans.* **1980**, 2509.
(23) Rosenberg, E. *Polyhedron* **1989**, *8*, 383.
(24) Rosenberg, E.; Novak, B.; Hajela, S. *Organometallics* **1989** *8*, 468.
(25) Rosenberg, E.; Novak, B. *Inorg. Synth.* **1990**, *26*, 328–334.
(26) King, R. B. *Organometallic Synthesis*; Academic Press: New York, 1965; Vol. 1, pp 114 and 151.
(27) Humphies, A. P.; Knox, S. A. R. *J. Chem. Soc., Dalton Trans.* **1975**, 1710.

band was dissolved in 140 mL of hexanes, and **5** was allowed to settle out over a period of about 2 h. The supernatant was then taken off, concentrated, and cooled to −20 °C, yielding larger red and smaller orange crystals of **2** (64.4 mg, 0.032 mmol, 10% yield). IR (CH_2Cl_2) ν(CO): 2082 (w), 2050 (s), 2008 (m), 1930 (w) cm^{-1}. ^1H NMR ($CDCl_3$) δ: 1.38 (9, s); 4.74 (5, s). Anal. Calcd for $C_{22}H_{14}O_{11}FeRu_3Hg$: C, 26.06; H, 1.48. Found: C, 26.33; H, 1.31.

Synthesis of (μ-H)(μ_3-η^2-C_2-*t*-Bu)$Os_3(CO)_9$. $Os_3(CO)_{12}$ (0.500 g 0.522 mmol) was dissolved in CH_2Cl_2 (300 mL) and CH_3CN (50 mL) in a 1.0-L three-neck round-bottom flask. The flask was fitted with a refluxing condenser with mercury bubbler and a pressure equalizing dropping funnel. A degassed solution of $(CH_3)_3NO{\cdot}2H_2O$ (0.160 g, 1.44 mmol) in CH_3CN (85 mL) was added to the dropping funnel. This solution was added dropwise to the refluxing osmium solution over a period of 1 h. Analytical thin-layer chromatography (silica gel with 80% hexanes, 10% CH_2Cl_2, and 10% CH_3CN as eluent) was used to confirm complete conversion to the bis-nitrile compound. The resulting pale yellow solution was filtered through a silica gel column (50 cm × 3.5 cm, 90% CH_2Cl_2 and 10% CH_3CN) two times and was rotary evaporated under vacuum to dryness, giving pale yellow crystals of $Os_3(CO)_{10}(CH_3CN)_2$. IR (CH_2Cl_2) ν(CO): 2077 (w), 2024 (s, sh), 2018 (vs), 1981 (s), 1958 (m) cm^{-1}.[10]

The yellow crystals from above were dissolved in CH_2Cl_2 (300 mL), and the solution was injected with 3,3-dimethyl-1-butyne (2.0 mL, 16.3 mmol). A color change from yellow to orange was noted in a varying amount of time (between 15 s and 20 min). Analytical thin-layer chromatography (eluents as above) was used to confirm complete conversion to the alkyne adduct, (μ_3-η^2-HC_2-*t*-Bu)$Os_3(CO)_{10}$. The solution was rotary evaporated under vacuum to dryness. The residue was taken up in octane (600 mL) and refluxed for 2 h. A color change from orange to yellow was noted. The yellow solution was allowed to cool, rotary evaporated under vacuum to 100 mL, passed through a silica gel column (25 cm × 3.5 cm, in heptane), one time, and then rotary evaporated under vacuum to dryness, giving (μ_3-η^2-C_2-*t*-Bu)(μ-H)$Os_3(CO)_9$ (0.298 g, 0.329 mmol) for a yield of 59.7% based on $Os_3(CO)_{12}$. IR (CH_2Cl_2) ν(CO): 2098 (w), 2072 (vs), 2049 (vs), 2017 (s), 1974 (w) cm^{-1}. ^1H NMR ($CDCl_3$) δ: −23.6 (s, 1), 1.44 (s, 9).

Synthesis of (μ_3-η^2-C_2-*t*-Bu)$Os_3(CO)_9$(μ-Hg)I. (μ-H)(μ_3-η^2-C_2-*t*-Bu)$Os_3(CO)_9$ (0.291 g, 0.328 mmol) was added to THF (150 mL) in a 300-mL three-neck round-bottom flask and degassed with CO. A 20% excess of ethanolic KOH (3.1 mL of 0.126 M, 0.393 mmol) was added dropwise over a 2-h period, at room temperature under a CO atmosphere. The solution was allowed to stir overnight. Infrared spectra of the reaction mixture indicated complete conversion to the anion. IR (THF) ν(CO): 2072 (w), 2049 (w), 2003 (m), 1994 (m), 1965 (s), 1939 (m) cm^{-1}. HgI_2 (0.542 g, 1.19 mmol) in THF (15 mL) was syringed into the anion solution and allowed to stir overnight. The solution was rotary evaporated and extracted three times with dichloromethane (5-mL portions) and the extracted solution run on preparative TLC plates (silica gel with 80% hexanes and 20% CH_2Cl_2 as eluent). The slowest moving of two bands was collected, giving (μ_3-η^2-C_2-*t*-Bu)$Os_3(CO)_9$(μ-Hg)I (0.232 g, 0.188 mmol, yield of 57.3%) IR (CH_2Cl_2) ν(CO): 2094 (w), 2067 (vs), 2054 (s), 2017 (s) cm^{-1}.

Synthesis of (μ_3-η^2-C_2-*t*-Bu)$(CO)_9Os_3$(μ_3-Hg)$Co(CO)_4$ (4). The $Co(CO)_4^-$ anion was prepared in THF by reductive cleavage of the dimer $[Co(CO)_4]_2$ by NaOH to form the sodium salt.[28] (μ_3-η^2-C_2-*t*-Bu)$(CO)_9Os_3$(μ-Hg)I (0.079 g, 0.064 mmol) was dissolved in THF (5.0 mL). $Co(CO)_4^-$ in THF (0.64 mL, 0.1 mmol) was injected into the solution, and analytical TLC (silica with 80% hexanes and 20% CH_2Cl_2 as eluent) indicated complete conversion. The solution was rotary evaporated, and the residue was dissolved in a minimum amount of dichloromethane. Preparative TLC (silica gel, eluent as above) gave one band, which was collected, giving (μ_3-η^2-C_2-*t*-Bu)$(CO)_9Os_3$(μ_3-Hg)$Co(CO)_4$ as pale yellow crystals (0.082 g, 0.063 mmol) for a yield of 98%. IR (CH_2Cl_2) ν(CO): 2070 (s), 2060 (vs), 2050 (vs), 2004 (vs) cm^{-1}. ^1H NMR ($CDCl_3$) δ: 1.41 (s). Anal. Calcd for $C_{19}H_9O_{13}Os_3CoHg$: C, 17.89; H, 1.71. Found: C, 18.13; H, 1.51.

Synthesis of (μ_3-η^2-C_2-*t*-Bu)$(CO)_9Os_3$(μ_3-Hg)$Mo(C_5H_5)(CO)_3$ (3). The $Mo(CO)_3(\eta^5$-$C_5H_5)^-$ anion was prepared by reductive cleavage of the dimer $[Mo(CO)_3(\eta^5$-$C_5H_5)]_2$ by Na/K alloy in THF to give the potassium salt.[27] (μ_3-η^2-C_2-*t*-Bu)$(CO)_9Os_3$(μ-Hg)I (0.210 g, 0.170 mmol) was dissolved in THF (25 mL). $Mo(CO)_3(\eta$-$C_5H_5)^-$ (6.9 mL of 0.05 M solution, 0.346 mmol) was injected into the solution. The solution was evaporated to dryness, dissolved in CH_2Cl_2, and eluted on preparative TLC plates (as above). One major band was eluted and collected, giving (μ_3-η^2-C_2-*t*-Bu)$(CO)_9Os_3$(μ_3-Hg)$Mo(CO)_3(\eta^5$-$C_5H_5)$ as pale yellow crystals (0.176 g, 0.130 mmol, yield 76.5%). IR (CH_2Cl_2) ν(CO): 2082 (w), 2053 (vs), 2024 (s), 2001 (s) 1890 (w) cm^{-1}. ^1H NMR ($CDCl_3$) δ: 5.34 (s, 5); 1.44 (s, 9). Anal. Calcd for $C_{23}H_{14}O_{12}MoOs_3Hg$: C, 20.46; H, 1.04. Found: C, 20.54; H, 0.84.

Preparation of [(μ-H)(μ_3-S)$(CO)_9Os_3]_2$(μ_4-Hg) (6). A 50-mL round-bottom flask is flame-dried under N_2 and then charged with HgI_2 (48.9 mg, 0.1078 mmol) and [(μ-H)$Os_3(CO)_9$(μ_3-S)][PPN][12] (300 mg, 0.2152 mmol). THF (10 mL) is added, and the solution is allowed to stir for 1 h. The product is isolated by removal of the solvent and run on a filtration silica gel column after dissolution in CH_2Cl_2. Removal of the solvent gives $(HOs_3(CO)_9S)_2Hg$ as a bright yellow powder in (164.8 mg, 0.0862 mmol) 80% yield. Anal. Calcd for $C_{18}H_2O_{18}S_2Os_6Hg$: C, 11.31; H, 0.11. Found: C, 11.37; H, 0.10. IR (CH_2Cl_2) ν(CO): 2103.2 (m), 2081.2 (vs), 2056.0 (vs), 2000.1 (s, br) cm^{-1}. ^1H NMR (CD_2Cl_2) δ: −22.26.

Crystal Structure Determinations. Crystals suitable for X-ray analysis for compounds **1**–**4** were obtained by recrystallization from hexanes at −20 °C. A suitable crystal of **6** was obtained by recrystallization from CH_2Cl_2 at −20 °C. Each crystal was attached with epoxy to a glass fiber, mounted in a brass pin, mounted in a goniometer head, and optically centered on an Enraf-Nonius CAD4 diffractometer. Cell constants and an orientation matrix for data collection for each compound were obtained from least-squares refinement of approximately 25 randomly selected reflections in the range $3° < \theta < 15°$. Details of the crystal data for all five compounds are given in Table I.

From systematic absences (indicated in Table I) and subsequent least-squares refinement of the structures, the choice of each of the respective space groups was confirmed. Data for each compound were collected by using the ω–2θ scan technique with variable scan rates of 1.3–8.3°/min in θ and ω and variable scan ranges calculated by θ scan width = 0.80 + 0.350 tan θ. Background measurements by using the moving crystal–moving counter technique were made at the beginning and end of each scan. Several standard reflections monitored every 120 minutes during data collection showed no appreciable loss in intensity; however, a decay correction was applied to the data as was an empirical absorption correction based on a series of ψ scans. Lorentz and polarization corrections were also applied to each data set.

The structures were solved by standard Patterson or direct methods and difference Fourier techniques (see Table I). Final refinement for each structure included anisotropic thermal parameters for the metal atoms and isotropic thermal parameters for all other atoms, except for compound **1** in which all atoms were refined anisotropically. Only those reflections with $F_o > 3\sigma(F_o)$ were used in the final full-matrix, least-square refinements. Scattering factors were taken from Cromer and Waber,[29] and anomalous dispersion effects were included for all atoms in F_c; the values of $\Delta f'$ and $\Delta f''$ were those of Cromer.[30] The highest peaks in the final difference Fourier techniques were positioned near to or within the metal atom framework or near to expected hydrogen atom positions. No attempt was made to locate hydrogen atoms except for those hydridic hydrogens attached to the osmium atoms in **6** whose positions were calculated by using HYDEX[22] and corroborated by the geometrical dispositions of the carbonyl groups. Final refinement parameters are listed in Table I.

We were unable to obtain crystals of **6** that were large enough to permit collection of high-angle data with sufficient intensity to allow the determination of Os–C and C–O distances with small errors. However, the geometry of the metal skeleton was our primary interest, so this is not viewed as a serious problem. The

(28) Edgell, W. F.; Lyford, J., IV. *Inorg. Chem.* **1970**, *9*, 1932.

(29) Cromer, D. T.; Waber, J. T. *International Tables for X-ray Crystallography*; Kynoch Press: Birmingham, England, 1974; Vol. IV, Table 2.2B.

(30) Cromer, D. T. *International Tables for X-ray Crystallography*; Kynoch Press: Birmingham, England, 1974; Vol. IV, Table 2.3.1.

10 highest peaks in the final difference Fourier techniques had electron densities ranging from 2.65 to 2.08 e/Å^3 but were very close to or within the metal skeleton at positions that made no chemical sense.

Acknowledgment. We gratefully acknowledge the National Science Foundation (Grant No. CHF 8711549) for support of this research.

Supplementary Material Available: Tables 7-11, listing positional parameters, and Tables 12-16, listing anisotropic thermal parameters, for **1**-**4** and **6** (13 pages); Tables 17-21, listing calculated and observed structure factors for **1**-**4** and **6** (188 pages). Ordering information is given on any current masthead page.

Cyclopentadienylmetal Trichloride Formation versus Metallocene Dichloride Formation in the Reactions of Silylated Cyclopentadienes with Zirconium and Hafnium Chlorides. Crystal Structure of (1,3-Bis(trimethylsilyl)cyclopentadienyl)titanium Trichloride

Charles H. Winter,* Xiao-Xing Zhou, Daniel A. Dobbs, and Mary Jane Heeg

Department of Chemistry, Wayne State University, Detroit, Michigan 48202

Received May 24, 1990

The reaction of zirconium and hafnium tetrachlorides with tris(trimethylsilyl)cyclopentadiene affords the monocyclopentadienyl complexes (1,3-bis(trimethylsilyl)cyclopentadienyl)zirconium trichloride (**1**, 73%) and (1,3-bis(trimethylsilyl)cyclopentadienyl)hafnium trichloride (**2**, 76%) in good isolated yields. The reaction of **1** with (1,3-bis(trimethylsilyl)cyclopentadienyl)lithium affords 1,1',3,3'-tetrakis(trimethylsilyl)zirconocene dichloride (74%). In contrast to the preparations of **1** and **2**, reaction of bis(trimethylsilyl)cyclopentadiene with zirconium and hafnium tetrachlorides affords 1,1'-bis(trimethylsilyl)zirconocene dichloride (**5**, 73%) and 1,1'-bis(trimethylsilyl)hafnocene dichloride (**6**, 76%). The reaction of (trimethylsilyl)cyclopentadiene with zirconium and hafnium tetrachlorides affords zirconocene dichloride (**7**, 91%) and hafnocene dichloride (**8**, 90%). The intermediacy of monocyclopentadienyl species in the preparation of the metallocene dichlorides is supported by the reaction of cyclopentadienylzirconium trichloride with (trimethylsilyl)cyclopentadiene to afford **7** (85%). Reaction of zirconium tetrachloride with 1 equiv of (trimethylsilyl)cyclopentadiene at 0 °C for 0.5 h affords **7** and cyclopentadienylzirconium trichloride in a (69 ± 2):(31 ± 2) ratio. The silyl group regiochemistry in **1** and **2** was established through an X-ray crystal structure determination of the titanium analogue (1,3-bis(trimethylsilyl)cyclopentadienyl)titanium trichloride (**3**). Complex **3** crystallizes in the orthorhombic space group *Pbnm* with a = 7.459 (3) Å, b = 11.799 (3) Å, c = 20.535 (3) Å, V = 1807.1 (9) Å^3, and Z = 4.

Introduction

The reactions of titanium tetrachloride with silylated cyclopentadienes have been extensively investigated.[1] It has been clearly established that titanium tetrachloride reacts with 1 equiv of the silylated cyclopentadiene to afford the cyclopentadienyltitanium trichloride as the sole product under all conditions. Hence, this procedure represents a particularly efficient route to monocyclopentadienyltitanium complexes. As part of studies relating to the preparation of highly soluble organometallic Lewis acids,[2] we required convenient syntheses of monocyclopentadienylzirconium and -hafnium trichlorides, where the cyclopentadienyl ligand contained one or more trimethylsilyl groups. On the basis of the results with titanium, the reactions of zirconium and hafnium tetrachlorides with silylated cyclopentadienes potentially offered an efficient route to monocyclopentadienylzirconium and -hafnium complexes. However, such reactions had not been described.[3] We now wish to report that these reactions are unexpectedly complex. Zirconium and hafnium complexes containing a single 1,3-bis(trimethylsilyl)-cyclopentadienyl ligand are easily accessed by the regiospecific silyl cleavage reaction of tris(trimethylsilyl)cyclopentadiene with the metal tetrachloride. In contrast, the related reactions of bis(trimethylsilyl)cyclopentadiene and (trimethylsilyl)cyclopentadiene with zirconium and hafnium tetrachlorides afford the metallocene dichlorides.

Results

Preparation of Complexes. Reaction of tris(trimethylsilyl)cyclopentadiene[4a] with zirconium and hafnium tetrachlorides in dichloromethane at ambient temperature for 3-4 h affords (1,3-bis(trimethylsilyl)cyclopentadienyl)zirconium trichloride (73%, **1**)[5] and (1,3-bis(trimethylsilyl)cyclopentadienyl)hafnium trichloride (76%, **2**) upon workup. Complexes **1** and **2** are isolated as moderately air-sensitive white powders, which are soluble

(1) (a) Cardoso, A. M.; Clark, R. J. H.; Moorhouse, S. *J. Chem. Soc., Dalton Trans.* **1980**, 1156. (b) Krebs, K. W.; Engelhard, H.; Nischk, G. E. Ger. Offen. 1,959,322. (c) Jutzi, P.; Seufert, A. *J. Organomet. Chem.* **1979**, *169*, 373. (d) Jutzi, P.; Kuhn, M. *Ibid.* **1979**, *173*, 221. (e) Abel, E. W.; Moorhouse, S. *Ibid.* **1971**, *29*, 227.

(2) Winter, C. H.; Kampf, J.; Zhou, X.-X. *Acta Crystallogr., Sect. C: Cryst. Struct. Commun.* **1990**, *C46*, 1231.

(3) For related literature, see: Schore, N. E. *J. Am. Chem. Soc.* **1979**, *101*, 7410. Llinâs, G. H.; Mena, M.; Palacios, F.; Royo, P.; Serrano, R. *J. Organomet. Chem.* **1988**, *340*, 37. Nief, F.; Mathey, F. *J. Chem. Soc., Chem. Commun.* **1988**, 770.

(4) (a) Jutzi, P.; Sauer, R. *J. Organomet. Chem.* **1973**, *50*, C29. (b) Miftakhov, M. S.; Tolstikov, G. A.; Lomakina, S. I. *Zh. Obshch. Khim.* **1976**, *46*, 2754. (c) Frisch, K. C. *J. Am. Chem. Soc.* **1953**, *75*, 6050.

(5) Duff, A. W.; Hitchcock, P. B.; Lappert, M. F.; Taylor, R. G.; Segal, J. A. *J. Organomet. Chem.* **1985**, *293*, 271.

0276-7333/91/2310-0210$02.50/0